Recombinant Expression and Initial Characterization of the Putative Human Enteric Ferric Reductase Dcytb†

Susanne Ludwiczek, Federico I. Rosell, Martin L. Ludwiczek, and A. Grant Mauk*

Department of Biochemistry and Molecular Biology and the UBC Centre for Blood Research, Life Sciences Centre, 2350 Health Sciences Mall, University of British Columbia, Vancouver, British Columbia V6T 1Z3, Canada

Received August 31, 2007; Revised Manuscript Received November 7, 2007

ABSTRACT: Recent studies of mutant mice with compromised ability to absorb dietary iron have identified involvement of two integral membrane proteins in the intestinal epithelial lining in iron uptake, a divalent metal ion transporter and a ferric reductase. The current study concerns the recombinant expression, purification, and initial spectroscopic characterization of a recombinant form of the human ferric reductase that was expressed and purified as the apoprotein from *Escherichia coli*. Reconstitution of the recombinant protein with ferriprotoporphyrin IX produced a red product with Soret (Fe^{3+}, λ_{max} 413.5 nm; Fe^{2+}, λ_{max} = 426 nm) and visible absorption maxima indicative of bisimidazole axial coordination. This observation was confirmed by electron paramagnetic resonance and magnetic circular dichroism spectroscopy. Titration of apo-Dcytb with ferriprotoporphyrin IX was consistent with the binding of two heme groups to the protein as predicted by the phylogenetic relationship of this protein to the cytochrome b_{561} family. Similar titrations and spectroscopic studies of two double variants of Dcytb, each lacking a pair of histidyl residues (H50 and H120 or H86 and H159) proposed on the basis of sequence alignment with other members of the cytochrome b_{561} family to provide axial ligands to bound heme, indicated that these variants were able to bind just one heme group each.

The predominant form of non-heme dietary iron is comprised of Fe^{3+} that is chelated to a variety of organic ligands, and various formulations of elemental iron are commonly taken orally to prevent or treat iron deficiency. Uptake of non-heme iron from the gut has recently been shown to be accomplished through the action of the divalent metal transporter DMT-1[1] that resides in the apical membranes of enterocytes (*1*, *2*). This discovery explains the fact that reduction of Fe^{3+} to Fe^{2+} accelerates iron uptake. McKie and colleagues have proposed that this reduction is achieved in the gut through the activity of a second enteric membrane protein, Dcytb, on the basis of studies of mutant mice that are deficient in this protein (*3*, *4*). The cDNA encoding Dcytb has been cloned from hypotransferrinemic mice, which exhibit a very high rate of iron absorption, and ferric reductase activity is increased in *Xenopus* oocytes and in cultured enterocytes that are transfected with this Dcytb cDNA (*5*). Dcytb protein and mRNA levels are highly elevated in mice maintained on an iron-deficient diet (*5*, *6*), in hemochromatosis (*7*−*10*), and under anemic (*11*, *12*) and hypoxic (*5*, *13*, *14*) conditions.

Further support for a role for Dcytb as the ferric enteric reductase is provided by the 45−50% sequence similarity of Dcytb to members of the cytochrome b_{561} family. Cytochrome b_{561} was originally observed in neuroendocrine vesicle membranes (*15*, *16*) and was long believed to be the only protein that supplied electron equivalents across membranes mediated by ascorbate as the electron donor (*17*−*19*). Recently, however, most eukaryotic cells have been found to possess similar membrane proteins (*20*). Although little is known about any of the other cytochrome b_{561} isoforms, sequence similarity suggests that all members of this family share a common motif, namely, six transmembrane helices, four conserved histidyl residues that provide axial ligands for two *b*-type heme groups that endow members of this family with electron transfer activity, and a binding site for ascorbate/monodehydroascorbate on both the cytosolic and extracellular sides of the protein (ALLVYRVFR in helix 1 and SLHSW in helix 4 of adrenal cytochrome b_{561}) (*5*, *20*−*22*). The principal physiological role of cytochromes b_{561} is regarded to be ascorbate-mediated transmembrane electron transport, and several members of this family have been linked to a ferric reductase activity (*23*). Although an essential role for Dcytb in iron absorption has been debated (*3*, *4*, *24*), the phylogenetic relationship of the protein to this family of reductases combined with its occurrence in the duodenal brush-border membrane has made Dcytb a protein of considerable interest and a potential target for therapeutic intervention.

Human Dcytb is a monomeric (MW 32 000, 286 amino acid residues), integral membrane protein. Of seven histidyl residues present in the sequence, residues H50, H86, H120,

† This work was supported by a Canadian Blood Services-Canadian Institute of Health Partnership Grant, Erwin Schrödinger Fellowships from the Austrian Science Fund (Projects J2441-B11 (S.L.) and J2430-B10 (M.L.L.)), and a Canada Research Chair (A.G.M.). The spectropolarimeter and spectrophotometer were funded by grants from the Canadian Foundation for Innovation to the UBC Laboratory of Molecular Biophysics and the Centre for Blood Research and operated with support of the Michael Smith Foundation for Health Research.

* To whom correspondence should be addressed. Phone: (604) 822-3719. Fax: (604) 822-6860. E-mail: mauk@interchange.ubc.ca.

[1] Abbreviations: Dcytb, enteric ferric reductase; DMT-1, divalent metal transporter.

10.1021/bi701793a CCC: $40.75
Published on Web 12/20/2007

and H159 are highly conserved and are thus likely heme ligand candidates. The corresponding His residues of adrenal cytochrome b_{561} have been proposed to provide two binding sites for heme, one at either end of the transmembrane stretch of the α-helices (*25*), and substitution (*23*) or chemical modification (*26*, *27*) of these residues impairs reduction of dehydroascorbate by that enzyme.

At present, characterization of Dcytb has been restricted primarily to genetic studies, with no report concerning isolation of the protein or characterization of its physical properties. The current study describes an efficient bacterial expression system for Dcytb and initial spectroscopic characterization of the wild-type and variant forms of the protein that provide evidence concerning the number of heme binding sites and identification of the axial ligands.

MATERIALS AND METHODS

Molecular Genetics. A cDNA library was prepared by reverse transcription from Caco-2 RNA (kindly provided by Professor Günter Weiss) that was derived from a human colonic adenocarcinoma cell line. Dcytb cDNA was cloned from this library by PCR with the sense primer 5′-gccatggagggctaccggc-3′ and the antisense primer 5′-cgcggatccttacatggtagatctctgccc-3′ into the refilled *Nco*I and the *Bam*HI restriction sites of the pET32b plasmid (Novagen) to create the plasmid 32D. Site-directed mutagenesis was performed with the QuikChange mutagenesis protocol (Stratagene) and the following primers to create the plasmids 32DCS, H50A/H120A, and H86A/H159A (complementary antisense primers are not shown): C76S, 5′-ccgtggacctggaaatccagcaagctcctgatg-3′; C130S, 5′-ggactgatagctgtcatatcctatttgttacagcttctt-3′; H50A, 5′-cactagagtttaactgggccccagtgctcatggtc-3′; H86A, 5′-cctgatgaaatccatcgctgcagggttaaatgc-3′; H120A, 5′-ccaatatgtacagtctggccagctgggttggactg-3′; H159A, 5′-gagcatttctcatgcccatagctgtttattctggaattg-3′. Plasmid DNA was isolated with the Qiagen plasmid mini kit, and the insertion of the point mutations was verified by sequence analysis.

Expression and Purification. The expression plasmids 32D, 32DCS, H50A/H120A, and H86A/H159A were transformed into the T7 RNA polymerase strain Rosetta pLysS (Novagen). Transformants were grown in M9 medium at 37 °C to an OD_{600} of 0.5. The temperature was lowered to 30 °C, and expression was induced with IPTG (0.5 mM). The cells were harvested by centrifugation 6 h after induction. The pellet was resuspended in phosphate buffer (pH 7.0, 20 mM) and frozen at −80 °C until further use.

The thawed cell suspension was incubated with DNAse I (2.5 μg/mL, Sigma-Aldrich) for 16−20 h at 4 °C and then centrifuged. The resulting pellet was washed with sodium phosphate buffer (pH 7, 20 mM) and solubilized in the same buffer containing SDS (0.1%) and sodium chloride (300 mM) (buffer A). Insoluble material was removed by centrifugation and filtration through a syringe filter (0.8 μm). The soluble fraction was loaded onto a HisPrep FF column (GE Healthcare) that had been equilibrated with buffer A. The protein eluted with sodium phosphate buffer (pH 7.4, 20 mM) containing imidazole (100 mM). The eluate (50 mL) was concentrated in a 30K Amicon concentrator and loaded onto a Sephadex G25 column (XK 26/10, 60 mL) that had been equilibrated with sodium phosphate buffer (pH 7, 20 mM) containing sucrosemonododecanoate (0.032%). The protein was digested with thrombin (37 U, Sigma-Aldrich) for 2 h at room temperature and concentrated by centrifugal ultrafiltration.

SDS−sample buffer (Tris buffer (pH 6.8, 60 mM) with glycerol (10%), SDS (3%), and bromphenol blue (0.005%)) was added to the protein, which was then loaded onto a 12.5% preparative SDS−polyacrylamide gel (Bio-Rad model 491 prep cell). Electrophoresis was performed overnight at room temperature in Laemmli buffer (Tris buffer (25 mM) containing glycine (190 mM) and SDS (0.1%)). Samples of the electrophoretic fractions were run on an SDS−polyacrylamide gel and stained with silver nitrate. Those fractions containing monomeric Dcytb were pooled, and the Laemmli buffer was exchanged for sodium phosphate buffer (pH 7, 20 mM) containing SDS (0.1%).

The protein concentration was determined either by the bicinchoninic acid (BCA) assay (Pierce Chemical Co.) according to the manufacturer's protocol or from the calculated (*28*) molar absorptivity at 280 nm (66 920 M^{-1} cm^{-1}). Hemin solutions were prepared for reconstitution of apo-Dcytb by dissolving hemin (Frontier Scientific, Logan, UT) in NaOH (0.1 M) and diluting to a final concentration of 1 mg/mL with sodium phosphate buffer (pH 7, 20 mM). Prior to reconstitution with heme, a sample of each apo-Dcytb preparation was titrated with heme to determine its heme binding capacity. The heme solution (0.95 equiv) was then added to the remainder of the preparation for spectroscopic analysis.

Electronic Absorption Spectroscopy. UV−vis spectra were recorded with a Cary model 6000i spectrophotometer at ambient temperature using quartz cells with a 1 cm path length. Reduction of Dcytb was accomplished with addition of excess solid sodium dithionite to the argon-purged protein solution in an anaerobic glovebox (Vacuum Atmospheres).

Titration of apo-Dcytb with heme was performed by incremental addition of a hemin solution (1 mg/mL) prepared as described above to a protein solution (2−5 μM) in sodium phosphate buffer (pH 7, 0.1% SDS). After each addition, the spectrum (240 to 800 nm) was recorded. Difference spectra of the protein sample titrated with heme and heme in buffer were calculated, and the absorbance intensity at the Soret maximum divided by the protein concentration was then plotted against the ratio of heme to protein.

Weighted differences in absorbance (ΔA_i, relative to that of the free protein) at each titration point i were calculated according to eq 1, and the result was fit to eq 2

$$\Delta A_i = A_{T,i} - A_{L,i} \quad (1)$$

$$\Delta A_i = A_0 + \Delta A_{max}(n[P]_{T,i} + [L]_{T,i} + K_d - \{(n[P]_{T,i} + [L]_{T,i} + K_d)^2 - 4n[P]_{T,i}[L]_{T,i}\}^{1/2})/2n[P]_{T,i} \quad (2)$$

(*29*−*31*) by a nonlinear least-squares analysis with the program SigmaPlot (Systat Software, San Jose) to obtain a dissociation constant (K_d) for formation of a 1:n protein−ligand complex. In this relationship, $A_{T,i}$ is the total absorbance at each titration point i, $A_{L,i}$ is the absorbance of the ligand (heme) as determined by titration of hemin solution against buffer in the absence of protein, ΔA_{max} is the total absorbance change upon saturation of the protein with ligand,

$[P]_{T,i}$ and $[L]_{T,i}$ are the total protein and total ligand concentrations, corrected for dilution, at each point *i*, and *n* is the number of ligand binding sites, which was assumed to be 2 for the wild-type protein and 1 for H50A/H120A and H86A/H159A. The dependence of ΔA_i on the [heme]/[protein] ratio was fit to eq 2, with $A_{L,i}$ corrected by the fraction of free ligand ($f_{[L]}$) using eqs 3 and 4.

$$\Delta A_i = A_{T,i} - A_{L,i} f_{[L]} \quad (3)$$

$$f_{[L]} = \frac{[L]_{T,i} - \frac{nA_{T,i}[P]_{T,i}}{A_{max}}}{[L]_{T,i}} \quad (4)$$

Circular Dichroism (CD) Spectroscopy. Circular dichroism spectra of protein solutions (~10 μM) were recorded at room temperature with a Jasco model J-720 spectropolarimeter. Far-UV CD spectra (190−250 nm) were obtained with a quartz cell (0.1 cm path length) and a scan rate of 50 nm/min. Near-UV and visible CD spectra (350−700 nm) were obtained in quartz cells (1 cm path length) with a scan rate of 100 nm/min. Spectra were recorded in triplicate and averaged. Secondary structure analysis was performed with the program K2d (*32*). Dcytb was reduced to the ferrous form by anaerobic addition of solid sodium dithionite.

Magnetic Circular Dichroism (MCD). Magnetic circular dichroism spectra were recorded at 20 °C with either a Jasco model J-720 spectropolarimeter (350−700 nm, 1 cm path length) or a Jasco model J-730 spectropolarimeter (800−2000 nm, 0.1 cm path length) equipped with an electromagnet (Alpha Magnetics, Hayward, CA) that generated a magnetic field of 1 T. For visible MCD spectroscopy, protein samples (10 μM) were exchanged into sodium phosphate buffer (pH 7, 20 mM) containing SDS (0.1%), while for NIR-MCD spectra, protein samples were exchanged into sodium phosphate buffers prepared in D_2O containing deuterated SDS. Dcytb was reduced to the ferrous form by anaerobic addition of solid sodium dithionite. MCD spectra were calculated from the difference between spectra obtained with parallel and antiparallel field orientations.

Electron Paramagnetic Resonance (EPR) Spectroscopy. EPR spectra were recorded at X-band (20 K) with a Bruker ESP 300E spectrometer fitted with an Oxford Instruments model 900 liquid helium cryostat, an Oxford Instruments ITC4 temperature controller, and a Hewlett-Packard model 5352B frequency counter. The microwave power (1.25 mW), microwave frequency (~9.44 GHz), modulation frequency (100 kHz), and amplitude (10 G) were as indicated. The protein samples contained 50% glycerol.

RESULTS

Expression and Purification. In developing the protocol for purification of recombinant Dcytb as described above, the final step of preparative SDS−PAGE was found to be essential to ensure separation of monomeric Dcytb from the cleaved tag and from aggregated Dcytb. During purification, the yield of protein decreased from about 65 mg/L of culture after the affinity chromatography to 3 mg/L after the SDS−PAGE. Most of this loss was attributable to aggregation of the protein. Substitution of Cys residues 76 and 130 with Ser decreased aggregation without changing the spectroscopic properties of the protein. The experiments reported below were, therefore, performed with protein in which both Cys residues were replaced with Ser, and this protein is referred to as wild-type Dcytb. The final yield for this form of the protein was ~10 mg of monomer/L of culture. The purity of the protein after each step of the purification protocol was evaluated by SDS−PAGE (Figure 1).

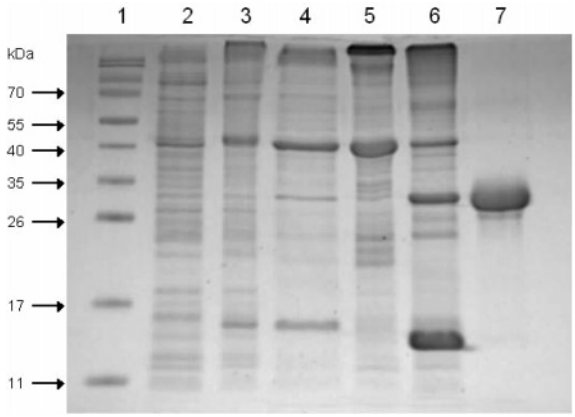

FIGURE 1: SDS−PAGE of recombinant Dcytb purification: lane 1, protein marker; lane 2, total protein extract of *Escherichia coli* cells carrying the plasmid 32DCS before induction with IPTG; lane 3, total protein extract after induction with IPTG; lane 4, isolated pellet; lane 5, protein extract after Ni^{2+}-affinity chromatography; lane 6, protein after thrombin cleavage; lane 7, pure protein after preparative SDS−PAGE. Equal amounts of protein were loaded into the SDS−sample buffer.

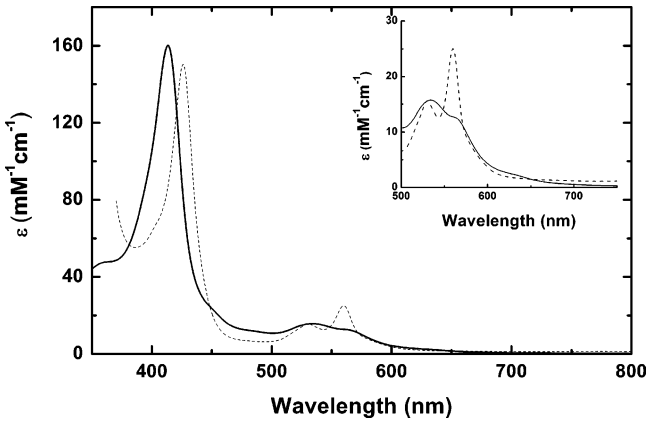

FIGURE 2: Electronic absorption spectra of purified Dcytb: spectra of oxidized (solid line) and reduced (dotted line) Dcytb reconstituted with heme (phosphate buffer, pH 7, 0.1% SDS).

Electronic Absorption and Far-UV CD Spectroscopy. Recombinant Dcytb expressed as described above was isolated as the apoprotein. Addition of a heme solution to the purified monomer produced a red protein with a Soret maximum at 413.5 nm, a broad β-band with $\lambda_{max} \approx 534$, and a shoulder at ~561 nm in the ferric form. Reduction with sodium dithionite shifted the Soret maximum to 426 nm and produced maxima at 560 and 530 nm as typically observed (*33*) for low-spin, six-coordinated heme proteins (Figure 2).

To evaluate the stoichiometry and affinity of heme binding, purified apo-Dcytb was titrated with heme, and the change in absorbance at the Soret maximum was monitored. In this titration (Figure 3), the increase in absorbance exhibits a break point at a heme:protein ratio of ~2 that is consistent with a stoichiometry of heme binding of 2:1. Numerical

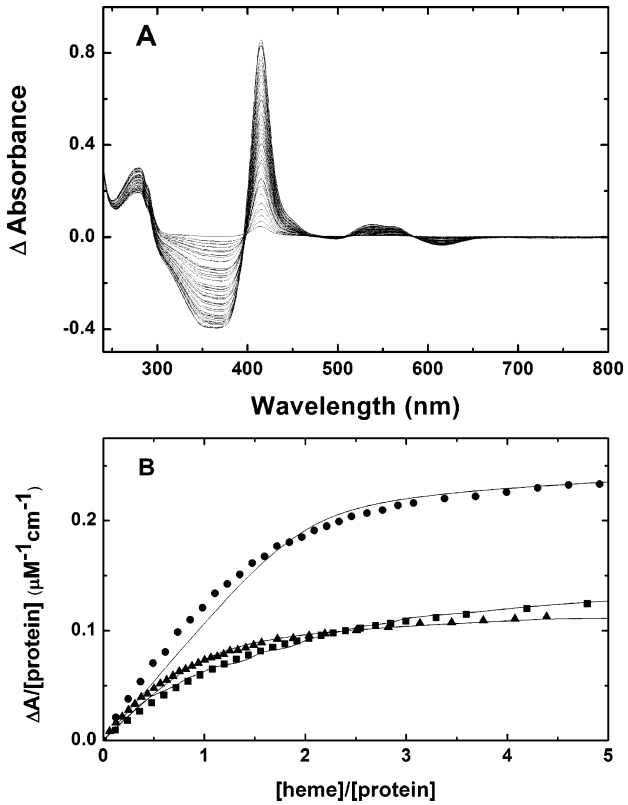

FIGURE 3: Titration of wild-type and variant Dcytb: (A) electronic difference spectra of apo-Dcytb titrated with heme, (B) titration of apo-Dcytb with heme as monitored at the Soret maximum [wild-type Dcytb (circles), H50A/H120A variant (triangles), and H86A/H159A variant (squares)]. The curves represent the fits of the data to eq 2 as described in the text.

analysis of these results as described above with a model that assumes two equivalent, noninteracting binding sites leads to an apparent dissociation constant, K_d, of $\sim 2 \times 10^{-7}$ M for each. Fitting the data to a model that assumes two inequivalent but noninteracting binding sites improves the quality of the fit to the data but leads to numerical values that are physically implausible. We attribute this observation to the inability of a manual titration to provide data of sufficient precision to withstand numerical analysis in terms of the number of adjustable parameters inherent in the more sophisticated two-site model. Additional challenges to any quantitative thermodynamic analysis of heme−protein binding interactions include the dimeric state of ferriprotoporphyrin IX in aqueous solution (*34*) and the relatively high protein concentration (2−5 μM) required to monitor heme binding. For this reason, we regard the K_d provided above as simply an indication of the order of magnitude of heme−protein complex stability.

Reconstitution of Dcytb with heme does not significantly alter the secondary structure as determined by far-UV CD spectroscopy experiments (Figure 4). The negative Cotton effects observed at 221 and 208 nm are typically observed for proteins with α-helical structure and are exhibited to a similar extent with and without heme bound. Estimation of the secondary structure from these spectra was consistent with 39% α-helical content for both the apo- and holoprotein. This helical content is similar to the value predicted by analysis of the sequence of Dcytb for secondary structure, suggesting that recombinant Dcytb purified by the procedure outlined above is folded correctly.

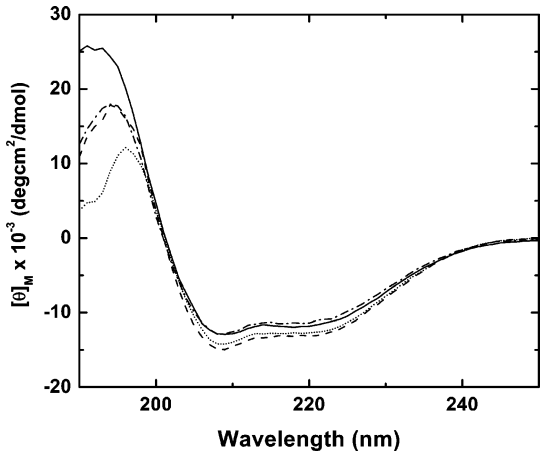

FIGURE 4: Far-UV CD spectroscopy: spectra of apo-Dcytb (solid line) and holo-Dcytb (dashed−dotted line) Dcytb and of the H50A/H120A (dashed line) and H86A/H159A (dotted line) variants (sodium phosphate buffer, pH 7, 0.1% SDS). Each spectrum is the average of three scans.

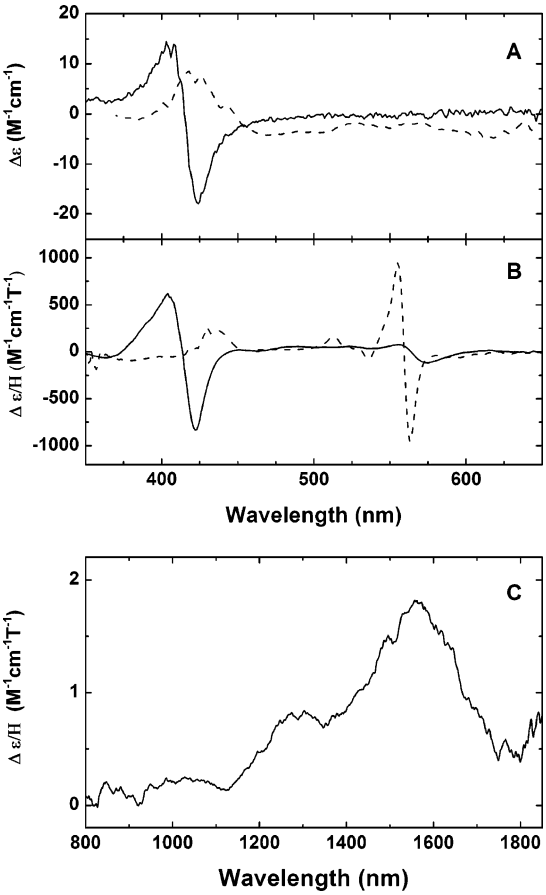

FIGURE 5: Soret CD, Soret MCD, and NIR MCD spectra of wild-type Dcytb reconstituted with heme: (A) visible CD spectra, (B) visible MCD spectra, and (C) near-infrared MCD spectra of Dcytb reconstituted with heme and recorded as described in the text. Spectra of oxidized (solid lines) and reduced (dashed lines) Dcytb are shown.

Circular Dichroism and Magnetic Circular Dichroism Spectroscopy. The Soret CD spectrum of oxidized Dcytb exhibits a bilobed line shape with a maximum at 406, a minimum at 424 nm, and a transition point at 413.5 nm (Figure 5). Reduction of the protein eliminated the bisignate shape to produce a maximum at 418 nm with a loss in intensity (Figure 5).

Table 1: Spectroscopic Properties of Wild-Type and Variant Forms of Recombinant Human Dcytb

		wild type		H50A/H120A		H86A/H159A	
		ox	red	ox	red	ox	red
UV−vis	Soret (nm)	413.5 (160)[a]	426 (150)	413.5 (93)	426 (92)	413 (123)	426 (106)
	α/β (nm)	534/∼563	530/560	535/∼563	531.5/560	533.5/∼562	530.5/560
Soret CD	λ_{max} (nm)	406 (14)	418 (6)	412 (4.4)	425 (3)	411 (3.8)	nd
		424 (−18)					
	crossover (nm)	415					
MCD	λ_{max} (nm)	404 (617)	430 (260)	406 (287)	431 (76)	406 (438)	555 (108)
		422 (−835)		421 (−395)		421 (−587)	
		556 (75)	555 (944)	556 (21)	555 (371)	556 (29)	
		574 (−118)	563 (−951)	575 (−57)	563 (−385)	574 (−91)	563 (−132)
	crossover (nm)	413.5/564	559.5	413/562	559.5	413/562.5	559.5
NIR MCD	λ_{max} (nm)	1564		1575		1580	
		1290		1375		1360	

[a] Molar absorptivities (mM^{-1} cm^{-1}) are indicated in parentheses.

The Soret MCD spectrum of oxidized Dcytb exhibits a pair of oppositely signed MCD bands of nearly equal amplitude at 404 and 422 nm that correspond to the absorption maximum at 413.5 nm, while a maximum at 430 nm is observed in the corresponding spectrum of the reduced protein. In the visible region, a positive band at 556 nm and a negative band at 574 nm were observed in the spectrum of the Fe^{3+}−Dcytb, while in the spectrum of the reduced protein, a pair of oppositely signed MCD bands at 555 and 563 nm are observed that correspond to the absorption band at 560 nm. In combination, these observations are consistent with a low-spin, six-coordinate Fe^{3+} heme center. The near-infrared MCD spectrum of Fe^{3+}−Dcytb exhibits maxima at 1564 and 1290 nm (Figure 5) and is also consistent with low-spin, six-coordinate heme (*35*−*37*).

Electronic and CD Spectroscopy of Putative Axial Ligand Variants. The phylogenetic conservation of four histidyl residues in the cytochrome b_{561} family combined with analysis of the amino acid sequence of Dcytb for anticipated secondary structure suggests that H50 and H120 comprise one pair of axial ligands binding heme iron and that H86 and H159 comprise the other. Therefore, two double variants were prepared by site-directed mutagenesis in which these residues were replaced by alanyl residues in a pairwise manner to produce the H50A/H120A and H86A/H159A variants. As for the wild-type protein studied above, both Cys residues were substituted with Ser residues in these two variants. Both variants were expressed at levels similar to that of the wild-type protein.

Far-UV CD spectra of these variants were closely similar to that of the wild-type protein, indicating that the secondary structure of Dcytb is not influenced significantly by these amino acid substitutions (Figure 4). Titration of the variants with heme resulted in apparent affinities for heme that are somewhat lower than that observed above for wild-type Dcytb. Specifically, the apparent K_d for heme binding to H50A/H120A is $5.8(8) \times 10^{-7}$ M and that for H86A/H159A is $1.6(1) \times 10^{-6}$ M (Figure 3). The titration curve for addition of heme to the H50A/H120A variant exhibited a break point at a heme:protein ratio of ∼1, consistent with the binding of just one heme prosthetic group to this protein. The affinity of the H86A/H159A variant for heme was sufficiently low under these conditions that a clear break point in the titration was not well defined. The molar absorptivities for both variants calculated on the basis of the total absorbance change upon saturation with heme (ΔA_{max}) derived from the fit to the titration data were decreased to 48% (H50A/H120A) and 64% (H86A/H159A variant) of the values obtained for wild-type Dcytb.

The Soret maximum of the H50A/H120A Fe^{3+}−Dcytb variant remained at 413.5 nm but shifted slightly for the H86A/H159A variant (Table 1). No change in the maxima of the Soret and α-bands was observed for either protein upon reduction with sodium dithionite. The EPR, MCD, and NIR MCD spectra of these variants displayed the same features as the wild-type protein but with diminished intensities (Table 1). Instead of the bisignate Soret CD spectrum observed for the wild-type Fe^{3+}−Dcytb, both of the corresponding spectra for the variants simply exhibited a maximum at 412 nm (H50A/H120A) or 411 nm (H86A/H159A).

EPR Spectroscopy. The EPR spectrum of wild-type Dcytb exhibits a set of signals at $g \approx 2.94$, 2.27, and 1.53 that is characteristic of low-spin heme iron with bisimidazole axial coordination (*38*) in which the imidazole side chains are nearly coplanar (*39*). This spectrum resembles that of a minor component in cytochrome b_{561} preparations that has been attributed to a "relaxed conformation of the protein with low ligation strain imposed by the native protein" (*40*), and it is the dominant low-spin species of Dcytb. However, the g_z peak in the spectrum of Dcytb is asymmetric with a shallower slope toward lower magnetic field, suggesting that an additional low-spin component with $g \approx 3.1$ could be present as is the case for cytochrome b_{561} (*40*). Nevertheless, a shoulder was not detected in this region even at lower modulation amplitude (2.5 vs 10 G), indicating that any additional species is at most a minor component of Dcytb.

At 4 K and higher microwave power (data not shown), the signals of the principal low-spin heme iron species of Dcytb become partially saturated to reveal a weak signal at $g_{max} = 3.67$. Although this feature could be assigned to a highly anisotropic, low-spin (HALS) heme iron and although this feature resembles that associated with the low-potential heme group in the spectrum of cytochrome b_{561} (*40*), the presence of the same weak signal is present in the spectrum of a heme solution used as a control. No other signals are evident at higher magnetic fields to confirm the presence of a HALS-type heme center, but the apparent absence of these signals could result from *g*-strain-induced line-broadening (*41*, *42*), masking by the residual signals from the principal low-spin heme species, or both.

The EPR spectrum of Dcytb also exhibits intense signals at $g \approx 6.06$ and 2.00 that are characteristic of axially symmetric, high-spin heme iron. While the observation of high-spin ferriheme signals is not expected for Dcytb, the presence of this species may be related to the purification method (as suggested for cytochrome b_{561} (*40*)) or to an artifact related to the detergent (*43*). The weak charge-transfer band at ~620 nm (Figure 2) indicates that the high-spin species is a minor component at ambient temperature.

DISCUSSION

Previous studies of Dcytb have emphasized genetic strategies that have provided some fundamental insights into the physiology and structural properties of this protein. Purification of Dcytb from tissue, however, has not been reported, presumably owing to difficulties related to purification of an integral membrane protein with an activity that is relatively nonspecific. Clearly, recombinant expression of Dcytb is the most appealing means of obtaining sufficient quantities of the protein for physical characterization. Expression of integral membrane proteins of mammalian origin in *Escherichia coli* is uncommon but not unknown (*44*−*46*). If such proteins do not insert into the bacterial membrane, they usually give rise to inclusion bodies from which correctly folded proteins cannot be prepared. The current success in expressing and solubilizing Dcytb from the insoluble fraction of an *E. coli* extract, therefore, is an exception to the rule. Interestingly, while this paper was in preparation, Liu et al. reported similar success in expressing bovine adrenal cytochrome b_{561} in the same strain of *E. coli* used in the current work (*47*). Evidently some feature of the sequences or structures of this family of integral membrane proteins allows their expression in a bacterial host.

Behavior of Recombinant Dcytb in Solution. The use of dilute SDS to solubilize recombinant Dcytb resulted from a survey of 64 detergents of varying charge and chain length. Dcytb was insoluble in most of these detergents. Of those detergents that could solubilize Dcytb to some extent, only Anzergent 3-12, Cymal-7, Foscholine-12, dodecyl-*N*,*N*′-dimethylglycine, and dodecyl-β-iminopropionic acid resulted in a solubilized protein that could bind heme (S. Ludwiczek, data not shown). In these cases, however, the stability of reconstituted Dcytb was limited. Although SDS is not generally used for refolding of insoluble recombinant proteins, it has been used successfully in NMR studies of the FXYD ion transporter (*48*), bullfrog substance P receptor (*49*), and M13 coat protein (*50*). The first indication that dilute SDS is compatible for use with Dcytb was the observation that the secondary structure estimated on the basis of the far-UV CD spectrum with the K2d program (*32*) is consistent with an α-helix content of 39%, a value essentially identical to the prediction of 37% α-helical content obtained from secondary structure prediction programs (*51*, *52*) that also suggest the presence of six transmembrane helices in the protein.

Further evidence for proper folding of Dcytb in this work is provided by retention of heme during standard SDS−PAGE as indicated by in-gel heme staining and by retention of heme during gel filtration chromatography in the presence of SDS (data not shown). Finally, electronic, Soret CD, MCD, and EPR are all compatible with the presence of six-coordinate, low-spin heme centers as expected on the basis of sequence alignment with cytochromes b_{561}. We note that proteolytic removal of the His_6 tag prior to addition of heme and subsequent analysis eliminate the possibility that heme binding and retention is simply an artifact arising from the presence of this sequence.

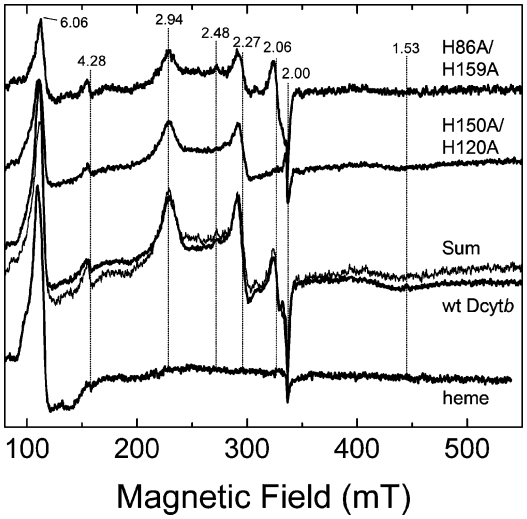

FIGURE 6: EPR spectra of oxidized Dcytb: X-band EPR spectra (20 K) of wild-type Dcytb (268 μM) and the variants H50A/H120A (277 μM) and H86A/H159A (190 μM) in 20 mM phosphate buffer, pH 7, 50% glycerol. Spectra have been normalized to a protein concentration of 268 μM. The sum of the spectra of the two variants and the spectrum of a heme solution obtained under identical conditions are placed adjacent to the spectrum of the wild-type protein to facilitate comparison.

Aggregation of the solublized protein during purification was diminished significantly, and the yield of purified enzyme increased 3-fold by replacing the two Cys residues present in the wild-type protein with Ser residues. Although Takeuchi et al. (*53*) reported that modification of the Cys residues in cytochrome b_{561} with 4,4′dithiopyridine changed the electronic properties of the protein, we found that the electronic, Soret CD, MCD, and EPR spectra for wild-type Dcytb and the variant lacking Cys residues were essentially identical (data not shown). Consequently, we used this variant as the control for spectroscopic studies and as the background for all subsequent mutagenesis in the current work.

Spectroscopic Studies. The electronic spectra of reduced and oxidized recombinant Dcytb (Figure 1) are indicative of six-coordinate, low-spin heme. Only histidine, lysine, methionine, or cysteine coordination is consistent with such a coordination environment, and the probability of His−Met coordination is diminished by the absence of a CT band at ~700 nm. As well, the UV−vis MCD spectra of Dcytb are typical of low-spin Fe^{3+}. The "S"-shaped band with a crossover at the Soret maximum is often observed in proteins with bishistidine coordination (*54*−*57*) or histidine−imidazole coordination (*58*). The maximum at 1564 nm in the NIR MCD spectrum is consistent with bishistidine, histidine−lysine, or methionine−histidinate coordination (*37*). This ambiguity can be reduced by consideration of the corresponding EPR spectrum (*37*, *59*). The g values ($g_z = 2.94$, $g_y = 2.27$, and $g_x = 1.53$; Figure 6) are indicative of a low-spin iron center and give rise (*38*, *60*) to a tetragonality (Δ/λ) of 3.27 and rhombicity (V/Δ) of 1.891 that place it in the "H-island" of the tetragonality vs rhombicity plot that is

characteristic of heme environments with two histidine residues coordinated with one or both imidazoles deprotonated (*61*).

As indicated above, the titration of apo-Dcytb with heme is consistent with binding of 2 equiv of heme to 1 equiv of Dcytb (Figure 3). Rigorous determination of the affinities of apoheme proteins for binding of heme is inherently problematic owing to the behavior of heme in aqueous solution and to the fact that the relatively high affinity with which heme binds to such proteins prevents their determination by direct titration at the concentrations of protein required for data collection. In other words, the affinity is usually so great that the stoichioimetry can be determined unambiguously but the affinity is numerically indeterminate (*62*). In the current case, the apparent affinity for heme is relatively low. We interpret this observation as indicating that the structural stability of Dcytb under the conditions employed in our work is sufficient to afford specific, spectroscopically informative binding of heme to the protein but insufficient to permit unambiguous quantitative determination of functional properties of the native protein. For this reason, we view the apparent affinities of the wild-type and variant forms of Dcytb for heme as lower limits of the true values that would be observed in a lipid bilayer environment if such values could be measured accurately.

The bisignate shape of the Soret CD spectrum of wild-type Dcytb that is absent from the corresponding spectra of the monoheme variants provides evidence of heme−heme interaction (*63*). Although a complex Soret CD spectrum of this type could result from distortion of a pyrrole ring from planarity with the remainder of the heme group or from distortion of the heme vinyl geometry (*64*, *65*), the most likely origin is exciton coupling (*66*) of the two heme centers.

The spectroscopic properties of the double variants H50A/H120A and H86A/H159A were studied to evaluate the proposal that each of these pairs of His residues provides axial ligands to a heme group. The shapes of the electronic, MCD, NIR MCD, and EPR spectra obtained for these variants following reconstitution with heme were similar to those of wild-type Dcytb, but they exhibited diminished intensity. The low intensity of the MCD spectrum obtained for the reduced H86A/H159A variant suggests that the some of the heme bound to this site may have dissociated from the protein upon reduction.

The present study describes an efficient bacterial expression system for the production of Dcytb, a protocol for purification of a monomeric form of the protein that binds heme to produce a product with the spectroscopic properties anticipated for the native protein and a means by which the functional properties of this protein may be evaluated. This potential has been demonstrated in part by the diminished heme binding capacity of variants lacking histidyl residues expected to serve as axial ligands to bound heme, thereby providing the first direct evidence concerning the identity of the axial ligands. The relatively low apparent affinity of the recombinant Dcytb for heme, the similarity of the EPR spectrum of Dcyt to the "relaxed" component of cytochrome b_{561}, and the observation of some high-spin component in the electronic spectrum of the protein, however, suggest that although the structure of Dcytb purified by the protocol described here is highly ordered, it is somewhat destabilized by the presence of dilute SDS that is currently essential for purification. This destabilization presumably accounts for the observation that Dcytb prepared as described here is readily reduced by dithionite to form the expected spectroscopic species but is not reduced by ascorbate (data not shown), a weaker reducing agent that is thought to be the physiological reductant. Heme bound to a destabilized form of Dcytb would experience a greater exposure to solvent, thereby increasing the dielectric constant of the heme binding environment and decreasing the reduction potential of the heme iron. To address this issue and eliminate any residual structural instability, future efforts will be directed to the reconstitution of recombinant Dcytb into nanodiscs as recently developed by Sligar and co-workers (*67*).

ACKNOWLEDGMENT

We thank Dr. Sabine Mair for helpful discussions and for studies of the reaction of Dcytb with ascorbate.

REFERENCES

1. Gunshin, H., Mackenzie, B., Berger, U. V., Gunshin, Y., Romero, M. F., Boron, W. F., Nussberger, S., Gollan, J. L., and Hediger, M. A. (1997) Cloning and characterization of a mammalian proton-coupled metal-ion transporter, *Nature 388*, 482−488.
2. Hentze, M. W., Muckenthaler, M. U., and Andrews, N. C. (2004) Balancing acts: Molecular control of mammalian iron metabolism, *Cell 117*, 285−297.
3. Gunshin, H., Starr, C. N., Direnzo, C., Fleming, M. D., Jin, J., Greer, E. L., Sellers, V. M., Galica, S. M., and Andrews, N. C. (2005) Cybrd1 (duodenal cytochrome *b*) is not necessary for dietary iron absorption in mice, *Blood 106*, 2879−2883.
4. Frazer, D. M., Wilkins, S. J., Vulpe, C. D., and Anderson, G. J. (2005) The role of duodenal cytochrome *b* in intestinal iron absorption remains unclear, *Blood 106*, 4413.
5. McKie, A. T., Barrow, D., Latunde-Dada, G. O., Rolfs, A., Sager, G., Mudaly, E., Mudaly, M., Richardson, C., Barlow, D., Bomford, A., Peters, T. J., Raja, K. B., Shirali, S., Hediger, M. A., Farzaneh, F., and Simpson, R. J. (2001) An iron-regulated ferric reductase associated with the absorption of dietary iron, *Science 291*, 1755−1759.
6. Collins, J. F. (2006) Gene chip analyses reveal differential genetic responses to iron deficiency in rat duodenum and jejunum, *Biol. Res. 39*, 25−37.
7. Herrmann, T., Muckenthaler, M., van der Hoeven, F., Brennan, K., Gehrke, S. G., Hubert, N., Sergi, C., Grone, H. J., Kaiser, I., Gosch, I., Volkmann, M., Riedel, H. D., Hentze, M. W., Stewart, A. F., and Stremmel, W. (2004) Iron overload in adult Hfe-deficient mice independent of changes in the steady-state expression of the duodenal iron transporters DMT1 and Ireg1/ferroportin, *J. Mol. Med. 82*, 39−48.
8. Ludwiczek, S., Theurl, I., Artner-Dworzak, E., Chorney, M., and Weiss, G. (2004) Duodenal HFE expression and hepcidin levels determine body iron homeostasis: Modulation by genetic diversity and dietary iron availability, *J. Mol. Med. 82*, 373−382.
9. Ludwiczek, S., Theurl, I., Bahram, S., Schumann, K., and Weiss, G. (2005) Regulatory networks for the control of body iron homeostasis and their dysregulation in HFE mediated hemochromatosis, *J. Cell Physiol. 204*, 489−499.
10. Muckenthaler, M., Roy, C. N., Custodio, A. O., Minana, B., deGraaf, J., Montross, L. K., Andrews, N. C., and Hentze, M. W. (2003) Regulatory defects in liver and intestine implicate abnormal hepcidin and Cybrd1 expression in mouse hemochromatosis, *Nat. Genet. 34*, 102−107.
11. Li, A. C., Warley, A., Thoree, V., Simpson, R. J., McKie, A. T., Kodjabashia, K., Thompson, R. P., and Powell, J. J. (2006) Immunolocalization of duodenal cytochrome *b*: A relationship with circulating markers of iron status, *Eur. J. Clin. Invest. 36*, 890−898.
12. Latunde-Dada, G. O., Vulpe, C. D., Anderson, G. J., Simpson, R. J., and McKie, A. T. (2004) Tissue-specific changes in iron metabolism genes in mice following phenylhydrazine-induced haemolysis, *Biochim. Biophys. Acta 1690*, 169−176.
13. Latunde-Dada, G. O., Van der Westhuizen, J., Vulpe, C. D., Anderson, G. J., Simpson, R. J., and McKie, A. T. (2002)

Molecular and functional roles of duodenal cytochrome B (Dcytb) in iron metabolism, *Blood Cells Mol. Dis. 29*, 356−360.
14. Takeuchi, K., Bjarnason, I., Laftah, A. H., Latunde-Dada, G. O., Simpson, R. J., and McKie, A. T. (2005) Expression of iron absorption genes in mouse large intestine, *Scand. J. Gastroenterol. 40*, 169−177.
15. Duong, L. T., and Fleming, P. J. (1982) Isolation and properties of cytochrome b_{561} from bovine adrenal chromaffin granules, *J. Biol. Chem. 257*, 8561−8564.
16. Duong, L. T., Fleming, P. J., and Russell, J. T. (1984) An identical cytochrome b_{561} is present in bovine adrenal chromaffin vesicles and posterior pituitary neurosecretory vesicles, *J. Biol. Chem. 259*, 4885−4889.
17. Srivastava, M., Duong, L. T., and Fleming, P. J. (1984) Cytochrome b_{561} catalyzes transmembrane electron transfer, *J. Biol. Chem. 259*, 8072−8075.
18. Wakefield, L. M., Cass, A. E., and Radda, G. K. (1986) Electron transfer across the chromaffin granule membrane. Use of EPR to demonstrate reduction of intravesicular ascorbate radical by the extravesicular mitochondrial NADH:ascorbate radical oxidoreductase, *J. Biol. Chem. 261*, 9746−9752.
19. Wakefield, L. M., Cass, A. E., and Radda, G. K. (1986) Functional coupling between enzymes of the chromaffin granule membrane, *J. Biol. Chem. 261*, 9739−9745.
20. Verelst, W., and Asard, H. (2003) A phylogenetic study of cytochrome b_{561} proteins, *Genome Biol. 4*, R38.
21. Perin, M. S., Fried, V. A., Slaughter, C. A., and Sudhof, T. C. (1988) The structure of cytochrome b_{561}, a secretory vesicle-specific electron transport protein, *EMBO J. 7*, 2697−2703.
22. Tsubaki, M., Nakayama, M., Okuyama, E., Ichikawa, Y., and Hori, H. (1997) Existence of two heme B centers in cytochrome b_{561} from bovine adrenal chromaffin vesicles as revealed by a new purification procedure and EPR spectroscopy, *J. Biol. Chem. 272*, 23206−23210.
23. Su, D., and Asard, H. (2006) Three mammalian cytochromes b_{561} are ascorbate-dependent ferrireductases, *FEBS J. 273*, 3722−3734.
24. Andrews, N. C., and Gunshin, H. (2005) Cybrd1 is not essential in mice, *Blood 106*, 4414.
25. Bashtovyy, D., Berczi, A., Asard, H., and Pali, T. (2003) Structure prediction for the di-heme cytochrome b_{561} protein family, *Protoplasma 221*, 31−40.
26. Njus, D., Wigle, M., Kelley, P. M., Kipp, B. H., and Schlegel, H. B. (2001) Mechanism of ascorbic acid oxidation by cytochrome b_{561}, *Biochemistry 40*, 11905−11911.
27. Kipp, B. H., Kelley, P. M., and Njus, D. (2001) Evidence for an essential histidine residue in the ascorbate-binding site of cytochrome b_{561}, *Biochemistry 40*, 3931−3937.
28. Gasteiger, E., Hoogland, C., Gattiker, A., Duvaud, S., Wilkins, M. R., Appel, R. D., and Bairoch, A. (2005) Protein identification and analysis tools on the ExPASy server, in *The Proteomics Protocols Handbook* (Walker, J. M., Ed.) pp 571−607, Humana Press, Totowa, NJ.
29. Erman, J. E., and Vitello, L. B. (1980) The binding of cytochrome *c* peroxidase and ferricytochrome *c*. A spectrophotometric determination of the equilibrium association constant as a function of ionic strength, *J. Biol. Chem. 255*, 6224−6227.
30. Mauk, M. R., Ferrer, J. C., and Mauk, A. G. (1994) Proton linkage in formation of the cytochrome c-cytochrome *c* peroxidase complex: electrostatic properties of the high- and low-affinity cytochrome binding sites on the peroxidase, *Biochemistry 33*, 12609−12609.
31. Ludwiczek, M. L., Heller, M., Kantner, T., and McIntosh, L. P. A secondary xylan binding site enhances the catalytic activity of a single domain family 11 glycoside hydrolase, *J. Mol. Biol. 373*, 337−354.
32. Andrade, M. A., Chacon, P., Merelo, J. J., and Moran, F. (1993) Evaluation of secondary structure of proteins from UV circular dichroism spectra using an unsupervised learning neural network, *Protein Eng. 6*, 383−390.
33. Smith, D. W., and Williams, R. J. P. (1970) The spectra of ferric haems and haemoproteins, *Struct. Bonding (Berlin) 7*, 1−45.
34. de Villiers, K. A., Kaschula, C. H., Egan, T. J., and Marques, H. M. (2007) Speciation and structure of ferriprotoporphyrin IX in aqueous solution: Spectroscopic and diffusion measurements demonstrate dimerization, but not mu-oxo dimer formation, *J. Biol. Inorg. Chem. 12*, 101−117.
35. Gadsby, P. M., Peterson, J., Foote, N., Greenwood, C., and Thomson, A. J. (1987) Identification of the ligand-exchange process in the alkaline transition of horse heart cytochrome *c*, *Biochem. J. 246*, 43−54.
36. Thomson, A. J., and Gadsby, P. M. (1990) A theoretical model of the intensity of the near-infrared porphyrin-to-iron charge-transfer transitions in low-spin iron(III) hemoproteins. A correlation between the intensity of the magnetic circular dichroism bands and the rhombic distortion parameter of iron, *J. Chem. Soc., Dalton Trans.* 1921−1928.
37. Cheesman, M. R., Greenwood, C., and Thomson, A. J. (1991) Magnetic circular dichroism of hemoproteins, *Adv. Inorg. Chem. 36*, 201−255.
38. Peisach, J., Blumberg, W. E., and Adler, A. (1973) Electron paramagnetic resonance studies of iron porphin and chlorin systems, *Ann. N.Y. Acad. Sci. 206*, 310−327.
39. Walker, F. A., Huynh, B.-H., Scheidt, W. R., and Osvath, S. R. (1986) Models of the cytochromes *b*. Effect of axial ligand plane orientation on the EPR and Mössbauer spectra of low-spin ferrihemes, *J. Am. Chem. Soc. 108*, 5288−5297.
40. Kamensky, Y., Liu, W., Tsai, A. L., Kulmacz, R. J., and Palmer, G. (2007) Axial ligation and stoichiometry of heme centers in adrenal cytochrome b_{561}, *Biochemistry 46*, 8647−8658.
41. Salerno, J. C. (1984) Cytochrome electron spin resonance line shapes, ligand fields, and components stoichiometry in ubiquinol-cytochrome *c* oxidoreductase, *J. Biol. Chem. 259*, 2331−2336.
42. Fahnenschmidt, M., Rau, H. K., Bittl, R., Haehnel, W., and Lubitz, W. (1999) Characterization of a de novo designed heme protein by EPR and ENDOR spectroscopy, *Chem.—Eur. J. 5*, 2327−2334.
43. Yruela, I., Garcia-Rubio, I., Roncel, M., Martinez, J. I., Ramiro, M. V., Ortega, J. M., Alonso, P. J., and Picorel, R. (2003) Detergent effect on cytochrome b_{559} electron paramagnetic resonance signals in the photosystem II reaction centre, *Photochem. Photobiol. Sci. 2*, 437−442.
44. Lockhart, E., Griffin, J. F., Chinn, N., Lavallie, E., and Buchan, G. (1996) The cloning, expression and purification of cervine interleukin 2, *Cytokine 8*, 603−612.
45. Quick, M., and Wright, E. M. (2002) Employing *Escherichia coli* to functionally express, purify, and characterize a human transporter, *Proc. Natl. Acad. Sci. U.S.A. 99*, 8597−8601.
46. Douglas, J. L., Trieber, C. A., Afara, M., and Young, H. S. (2005) Rapid, high-yield expression and purification of Ca^{2+}-ATPase regulatory proteins for high-resolution structural studies, *Protein Expression Purif. 40*, 118−125.
47. Liu, W., Rogge, C. E., Kamensky, Y., Tsai, A.-L., and Kulmacz, R. J. (2007) Development of a bacterial system for high yield expression of fully functional adrenal cytochrome b_{561}, *Protein Expression Purif. 56*, 145−152.
48. Crowell, K. J., Franzin, C. M., Koltay, A., Lee, S., Lucchese, A. M., Snyder, B. C., and Marassi, F. M. (2003) Expression and characterization of the FXYD ion transport regulators for NMR structural studies in lipid micelles and lipid bilayers, *Biochim. Biophys. Acta 1645*, 15−21.
49. Perrine, S. A., Whitehead, T. L., Hicks, R. P., Szarek, J. L., Krause, J. E., and Simmons, M. A. (2000) Solution structures in SDS micelles and functional activity at the bullfrog substance P receptor of ranatachykinin peptides, *J. Med. Chem. 43*, 1741−1753.
50. Papavoine, C. H., Konings, R. N., Hilbers, C. W., and van de Ven, F. J. (1994) Location of M13 coat protein in sodium dodecyl sulfate micelles as determined by NMR, *Biochemistry 33*, 12990−12997.
51. Lao, D. M., Okuno, T., and Shimizu, T. (2002) Evaluating transmembrane topology prediction methods for the effect of signal peptide in topology prediction, *In Silico Biol. 2*, 485−494.
52. Rost, B., Yachdav, G., and Liu, J. (2004) The PredictProtein server, *Nucleic Acids Res. 32*, W321−W326.
53. Takeuchi, F., Hori, H., and Tsubaki, M. (2005) Selective perturbation of the intravesicular heme center of cytochrome b_{561} by cysteinyl modification with 4,4′-dithiodipyridine, *J. Biochem. (Tokyo) 138*, 751−762.
54. Cox, M. C., Le Brun, N., Thomson, A. J., Smith, A., Morgan, W. T., and Moore, G. R. (1995) MCD, EPR and NMR spectroscopic studies of rabbit hemopexin and its heme binding domain, *Biochim. Biophys. Acta 1253*, 215−223.
55. Morgan, W. T., and Vickery, L. E. (1978) Magnetic and natural circular dichroism of metalloporphyrin complexes of human and rabbit hemopexin, *J. Biol. Chem. 253*, 2940−2945.
56. Vickery, L., Nozawa, T., and Sauer, K. (1976) Magnetic circular dichroism studies of low-spin cytochromes. Temperature depen-

dence and effects of axial coordination on the spectra of cytochrome *c* and cytochrome b_5, *J. Am. Chem. Soc. 98*, 351−357.
57. Dolinger, P. M., Kielczewski, M., Trudell, J. R., Barth, G., Linder, R. E., Bunnenberg, E., and Djerassi, C. (1974) Magnetic circular dichroism studies. XXV. A preliminary investigation of microsomal cytochromes, *Proc. Natl. Acad. Sci. U.S.A. 71*, 399−403.
58. Vickery, L., Nozawa, T., and Sauer, K. (1976) Magnetic circular dichroism studies of myoglobin complexes. Correlations with heme spin state and axial ligation, *J. Am. Chem. Soc. 98*, 343−350.
59. Gadsby, P. M., and Thomson, A. J. (1990) Assignment of the axial ligands of ferric ion in low-spin hemoproteins by near-infrared magnetic circular dichroism and electron paramagnetic resonance spectroscopy, *J. Am. Chem. Soc. 112*, 5003−5011.
60. Taylor, C. P. (1977) The EPR of low spin heme complexes. Relation of the t2g hole model to the directional properties of the g tensor, and a new method for calculating the ligand field parameters, *Biochim. Biophys. Acta 491*, 137−148.
61. Walker, F. A. (2004) Models of the bis-histidine-ligated electron-transferring cytochromes. Comparative geometric and electronic structure of low-spin ferro- and ferrihemes, *Chem. Rev. 104*, 589−615.
62. Laskowski, M., Jr., and Finkenstadt, W. R. (1972) Study of protein-protein and of protein-ligand interactions by potentiometric methods, *Methods Enzymol. 26 PtC*, 193−277.
63. Myer, Y. P. (1978) Circular dichroism spectroscopy of hemoproteins, *Methods Enzymol. 54*, 249−284.
64. Blauer, G., Sreerama, N., and Woody, R. W. (1993) Optical activity of hemoproteins in the Soret region. Circular dichroism of the heme undecapeptide of cytochrome *c* in aqueous solution, *Biochemistry 32*, 6674−6679.
65. Mauk, M. R., Rosell, F. I., Lelj-Garolla, B., Moore, G. R., and Mauk, A. G. (2005) Metal ion binding to human hemopexin, *Biochemistry 44*, 1864−1871.
66. Hsu, M. C., and Woody, R. W. (1971) The origin of the heme Cotton effects in myoglobin and hemoglobin, *J. Am. Chem. Soc. 93*, 3515−2355.
67. Nath, A., Atkins, W. M., and Sligar, S. G. (2007) Applications of phospholipid bilayer nanodiscs in the study of membranes and membrane proteins, *Biochemistry 46*, 2059−2069.

BI701793A